Chemical Science

ROYAL SOCIETY OF CHEMISTRY

EDGE ARTICLE

View Article Online
View Journal | View Issue

Cite this: *Chem. Sci.*, 2022, **13**, 14090

All publication charges for this article have been paid for by the Royal Society of Chemistry

Received 28th July 2022
Accepted 5th November 2022

DOI: 10.1039/d2sc04192h

rsc.li/chemical-science

Controlled monodefluorination and alkylation of C(sp^3)–F bonds by lanthanide photocatalysts: importance of metal–ligand cooperativity†‡

Amy E. Kynman,[ab] Luca K. Elghanayan,[a] Addison N. Desnoyer,[a] Yan Yang,[c] Laurent Sévery,[a] Andrea Di Giuseppe,[a] T. Don Tilley,[a] Laurent Maron *[c] and Polly L. Arnold *[ab]

The controlled functionalization of a single fluorine in a CF_3 group is difficult and rare. Photochemical C–F bond functionalization of the sp^3-C–H bond in trifluorotoluene, $PhCF_3$, is achieved using catalysts made from earth-abundant lanthanides, $(Cp^{Me4})_2Ln(2\text{-}O\text{-}3,5\text{-}^tBu_2\text{-}C_6H_2)(1\text{-}C\{N(CH)_2N(^iPr)\})$ (Ln = La, Ce, Nd and Sm, $Cp^{Me4} = C_5Me_4H$). The Ce complex is the most effective at mediating hydrodefluorination and defluoroalkylative coupling of $PhCF_3$ with alkenes; addition of magnesium dialkyls enables catalytic C–F bond cleavage and C–C bond formation by all the complexes. Mechanistic experiments confirm the essential role of the Lewis acidic metal and support an inner-sphere mechanism of C–F activation. Computational studies agree that coordination of the C–F substrate is essential for C–F bond cleavage. The unexpected catalytic activity for all members is made possible by the light-absorbing ability of the redox non-innocent ligands. The results described herein underscore the importance of metal–ligand cooperativity, specifically the synergy between the metal and ligand in both light absorption and redox reactivity, in organometallic photocatalysis.

Photoredox catalysis is a powerful synthetic method for the functionalization of inert molecules using single electron transfer (SET) reactivity[1–3] under irradiation with visible light.[4] This has enabled challenging transformations under mild conditions including C–H activation,[5–7] radical cross-coupling,[8–11] and the valorization of lignin.[12,13] However, detailed mechanistic studies of photoredox systems are difficult due to their inherent complexity and the short lifetimes of photoexcited intermediates.

Many lanthanides are more abundant in the environment than copper and their salts are less toxic than those of iron, so their potential for applications in catalysis merits exploration.[14–17] In 1990, divalent Sm, Eu, and Yb complexes $Ln(Cp^*)_2$ ($Cp^* = C_5Me_5$), were shown to more efficiently cleave vinylic C–F bonds when photolyzed, stoichiometrically forming Ln(III) halide complexes, and suggesting the value of increasing the reducing power of the Ln^{II} excited state.[18] Subsequently, analogous reactions to cleave the weaker C–Cl and C–Br bonds could be made catalytic in Ln(II) halide (Ln = Sm, Eu, Yb), under near UV-photolysis conditions, by the addition of sacrificial reductant such as Zn or Al.[19,20] The addition of simple donor ligands enabled benzylic C–Cl cleavage by Eu^{II} under blue light irradiation.[21] The addition of an organic photocatalyst or a photo-absorbing substrate to Lewis acidic LnX_3 salts (X = halide, triflate) has also been used to enhance the catalysis.[22] Ln centers (Ln = Nd, Dy, Lu) with light-absorbing ligands such as porphyrins or phthalocyanins have been used to stoichiometrically dechlorinate phenols.[23]

Few reports of lanthanide photoredox catalysis exist with Ce^{III} complexes receiving the most attention. Ce possesses both an accessible III/IV redox couple and an allowed excitation from the $4f^1$ ground state to the $5d^1$ excited state, which can give rise to luminescent behaviour. It is also the cheapest and most readily isolated of the rare earths, offering a promising alternative to current precious metal photocatalysts.

Building on the pioneering work on stoichiometric photoluminescent Ce chemistry,[24,25] in 2015 Schelter and co-workers demonstrated the utility of Ce^{III} in photocatalysis.[26,27] Their Ce^{III} amido complexes were catalysts for chlorine atom abstraction from benzyl chloride (Fig. 1, top), with both $NaN(SiMe_3)_2$ and additional Ce^0 required for turnover.[28]

[a]*Department of Chemistry, University of California, Berkeley, Berkeley, CA 94720-1460, USA. E-mail: pla@berkeley.edu*

[b]*Chemical Sciences Division, Lawrence Berkeley National Laboratory, Berkeley, CA 94720, USA*

[c]*LPCNO, Université de Toulouse, 135 Avenue de Rangueil, 31077 Toulouse, France. E-mail: laurent.maron@irsamc.ups-tlse.fr*

† This paper is dedicated to the memory of Luca Elghanayan (2002–2022), who made important contributions to this research.

‡ Electronic supplementary information (ESI) available: Additional experimental, computational, and crystallographic data (PDF). Raw datasets are in the open data archive doi: https://10.17632/8bx8zxbdgm.1. CCDC 2121204–2121215 and 2217133. For ESI and crystallographic data in CIF or other electronic format see DOI: https://doi.org/10.1039/d2sc04192h.

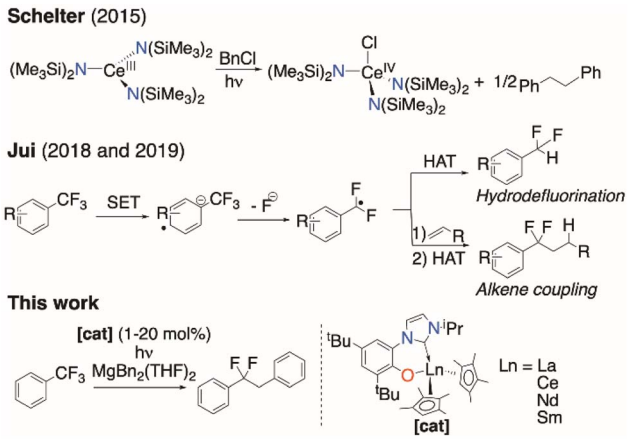

Fig. 1 Previous examples of photocatalytic C–X (X = halide) bond cleavage, and this work.

They proposed an inner-sphere mechanism involving Ce···$ClCR_3$ adduct formation that provides an additional thermodynamic driving force to a bond cleavage that was otherwise out of range of the reducing power of the Ce excited state. A more sterically congested Ce^{III} tris(guanidinate) operates *via* an outer-sphere single electron transfer (SET) mechanism to cleave aryl iodides,[28] highlighting the mechanistic diversity that is possible in these systems.[29]

To date, ligands that support lanthanide-centered photocatalysts have been limited to halides, pseudohalides, and simple N-donors.[30,31] No organometallic lanthanide photocatalyst has yet been reported that combines the photoexcitable Ce cation with multidentate, tunable ligands. We have developed organometallic lanthanide complexes as sustainable catalysts,[16,17,32,33] and considered that those capable of forming an inner-sphere adduct, and absorbing light, could achieve the unusual and difficult, selective catalytic conversion of strong sp^3 C–F bonds.

Fluorine forms the strongest single bond to carbon and the C–F bond is *ca.* 25 kcal mol^{-1} stronger than the C–Cl bond in monohaloalkanes, and the C–H bond in alkanes.[34] The selective activation and functionalization of C–F bonds is important, both due to the high bioaccumulation and toxicity of many perfluorinated compounds,[35] and the utility of fluorinated pharmaceuticals.[36] However, stoichiometric C(sp^3)–F bond activation reactions are rare.[37–40] In particular, it is difficult to facilitate the controlled cleavage of a single C–F bond as the C(sp^3)–F bond strength decreases as each F is removed and the remaining C–F bonds lengthen.[41,42]

This obstacle makes a radical methodology more attractive.[43–49] Jui and co-workers have demonstrated that some common photocatalysts can selectively activate a single C–F bond to form the putative $ArCF_2^{\bullet}$ radical, which can either be quenched directly *via* H atom transfer (HAT), or coupled with an alkene followed by HAT to generate difluoroalkanes (Fig. 1, middle).[50,51] Gschwind and König have shown the photochemical functionalization of electron-poor trifluoromethylarenes.[52] Nishimoto and Yasuda have described related C–F coupling protocols of perfluoroalkylarenes using tin reagents and an iridium photocatalyst.[53]

Here we show how selective, catalytic C–F bond functionalization can be achieved using a new family of Ln^{III} compounds supported by a light-absorbing aryloxide-tethered N-heterocyclic carbene, Cp^{Me4}, and pseudohalide ligands (Fig. 1, lower). We show that visible light-irradiated Ce complexes can selectively abstract a single fluoride from $PhCF_3$ and catalyze its alkylation by MgR_2 to afford $PhCF_2R$. The $PhCF_2^{\bullet}$ can also be quenched to selectively form $PhCF_2H$ or further alkylated *via* coupling with an alkene or other metal alkyls. We use combined experiment and density functional theory (DFT) computations to show the importance of coordination of the fluorinated substrate to the Lewis acidic metal in C–F activation, and the utility of the ligand in enabling photoredox catalysis for other lanthanide congeners.

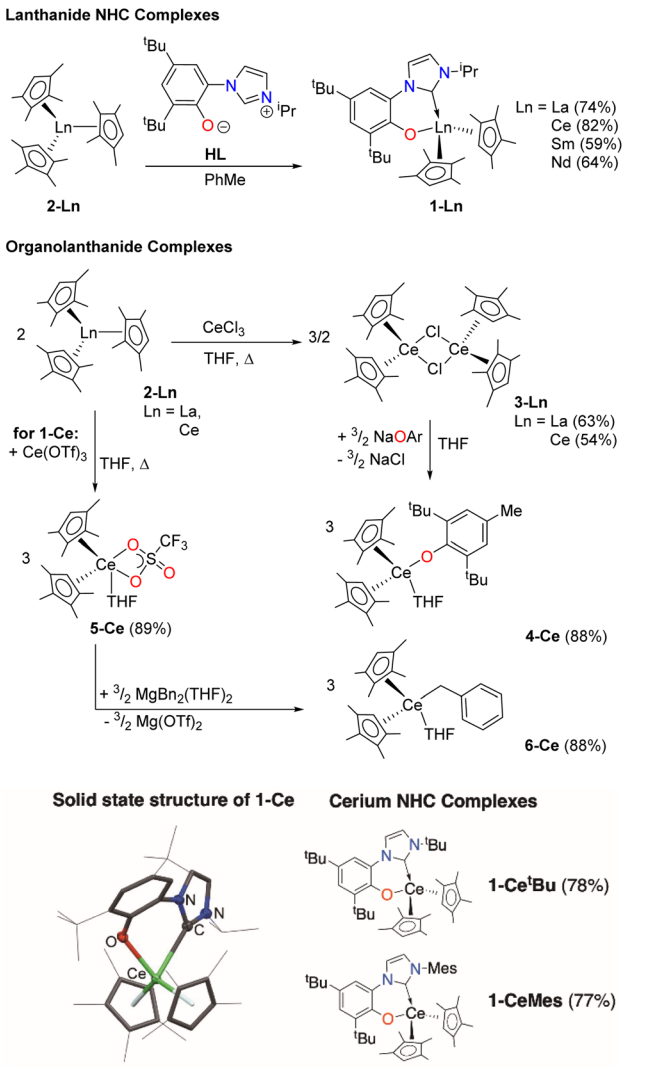

Scheme 1 Syntheses of the complexes examined for C–F bond functionalization in this work (upper) and the solid-state structure of **1-Ce**, H omitted for clarity, alongside the ligand variations studied for **1-Ce** (lower).

Synthesis and light absorption studies of the complexes

We first made the Ce complex $(Cp^{Me4})_2Ce(\mathbf{L})$ (**1-Ce**, Cp^{Me4} = C_5Me_4H), where **L** is the bidentate aryloxide-N-heterocyclic carbene (NHC) ligand [2-*O*-3,5-^{t}Bu$_2$-C$_6$H$_2$(1-C{N(CH)$_2$N(^{i}Pr)})], Scheme 1, top.[16,17]

This ligand has two important characteristics that could open up photoredox catalysis to typically redox-innocent lanthanides with other electronic configurations than Ce. Like some planar aromatic heterocycles,[54–56] the aryloxy-NHC **L** absorbs visible light when bound as a rigid bidentate ligand. The aryloxide group also has the potential to engage in one-electron redox chemistry by forming a phenoxy ligand radical.[57–59] To probe the roles of both metal and ligand, we prepared differently substituted aryloxy-NHC ligand adducts with a variety of electronic and steric profiles[16] $(Cp^{Me4})_2Ce(\mathbf{L^{Mes}})$ (**1-CeMes**) L^{Mes} = 2-*O*-3,5-^{t}Bu$_2$-C$_6$H$_2$(1-C{N(CH)$_2$N(Mes)}) and $(Cp^{Me4})_2Ce(\mathbf{L^{tBu}})$ (**1-Ce^{t}Bu**) L^{Mes} = 2-*O*-3,5-^{t}Bu$_2$-C$_6$H$_2$(1-C{N(CH)$_2$N(^{t}Bu)}), Scheme 1, bottom, and a series of Ln^{III} complexes – f^0 La, f^2 Nd and f^5 Sm analogues $(Cp^{Me4})_2Ln(\mathbf{L})$ (**1-La**, **1-Nd** and **1-Sm**), $Ln(Cp^{Me4})_3$ (**2-La** and **2-Ce**) $[(Cp^{Me4})_2Ln(\mu\text{-}Cl)]_2$,[24] (**3-La** and **3-Ce**), $(Cp^{Me4})_2Ce(OAr)$ (**4-Ce**, where OAr = *O*-2,6-^{t}Bu$_2$-4-Me-C$_6$H$_2$),[60] $(Cp^{Me4})_2Ce(OTf)(THF)$ (**5-Ce**),[61] and $(Cp^{Me4})_2Ce(Bn)(THF)$ (**6-Ce**, Bn = CH$_2$Ph),[62,63] Scheme 1, middle. All new complexes were fully characterized, see ESI.‡

The UV-Vis spectrum of the f^1 molecule **1-Ce** is shown in Fig. 2, overlaid with that of the f^0 congener **1-La**, proligand **HL**, and **1-CeMes**. All **1-Ln** luminesce under visible light excitation, with absorptions in the range 350–510 nm, see Fig. S23–S26‡ for the other **1-Ln** spectra, and the excitation and emission spectra of **1-Ce**. The two absorption maxima displayed by **1-CeMes** are shifted closer in energy to each other, while the magnitude of the ligand-centered absorption of **1-Ce^{t}Bu** (Fig. S24‡) is larger than that of **1-Ce** and **1-CeMes**. This suggests the possibility for further catalyst optimization by generating a broader envelope of light absorption or improving quantum yield.

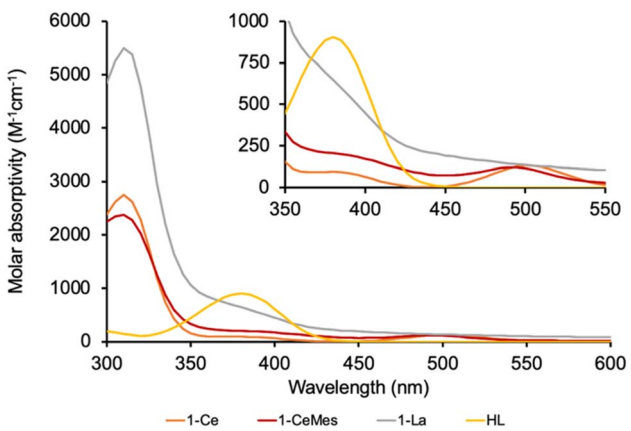

Fig. 2 The absorption spectra of **1-Ce**, **1-CeMes**, **1-La** and proligand HL. The absorption spectrum for the *tert*-Bu substituted analogue **1-Ce^{t}Bu**, is also shown overlayed in the ESI.‡ The computed spectrum of **1-Ce** using TD-DFT is included in the ESI.‡

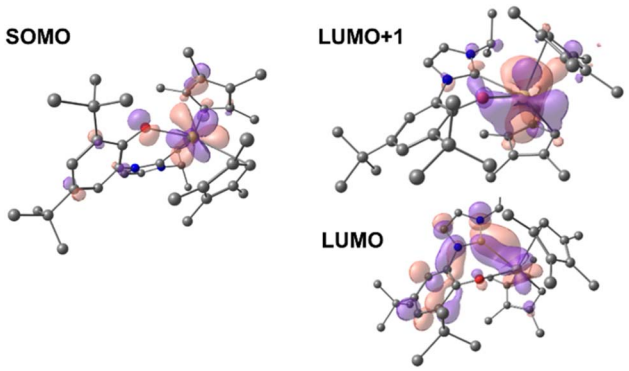

Fig. 3 Depictions of the TD-DFT-calculated SOMO (left) and LUMO+1 (right, upper) and LUMO (right, lower) orbitals of **1-Ce**.

TD-DFT analysis of the frontier orbitals involved in the light absorption

Time-dependent DFT (TD-DFT; B3PW91) calculations were performed on both **1-Ce** and **1-La** to explore the orbitals involved in their photoexcitation. The calculated and experimental absorption spectra agree well for **1-Ce** (see Fig. S134‡). As expected, the SOMO of **1-Ce** is comprised predominately of 4f character with minor orbital contributions from the aryloxide ligand (Fig. 3).

The absorption at 504 nm corresponds mainly to the SOMO–LUMO and SOMO–LUMO+1 transitions (see ESI‡ for the details of the states and the other frontier MOs). This is an excitation from an f-orbital into either the Ce–NHC or Ce–Cp^{Me4} orbitals. The LUMO+1 is calculated to be a Ce-based (89%) hybrid of f- and d-orbitals (54% 5d and 46% 4f mixture) with no significant contributions from the ligands (11%). Notably, the LUMO, which also contributes to the calculated absorbance bands at 504 and 384 nm, is primarily of p-character and delocalized over both the aromatic ring and NHC moiety of the ligand **L**.

In the case of **1-La**, the HOMO was calculated to be composed of significant π symmetry orbital contributions from both the Cp^{Me4} and **L** ligands, Fig. 4. As expected for a formally f^0 complex, there is no appreciable contribution from any La-based orbital to the HOMO. However, the LUMO+1 is predominately d-character (63% 5d and 23% 4f). TD-DFT predicts that

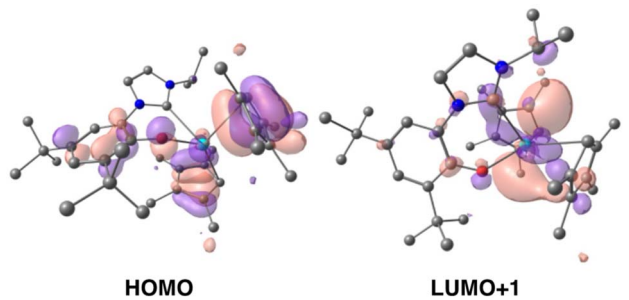

Fig. 4 Depictions of the TD-DFT-calculated HOMO (left) and LUMO+1 (right) for **1-La**.

the transition from HOMO to LUMO+1 results in a band at 325 nm. For both **1-La** and **1-Ce**, transitions are calculated in the higher energy region (between 320 and 390 nm) that involve π-type orbitals (Ln–Cp^{Me4}, Ln–NHC).

Cyclic voltammetry and the excited state reduction potential of 1-Ce

The Rehm–Weller formalism is often used to estimate the excited state reduction potential ($E_{1/2}$*) of photocatalysts.[2,28] Excitation of a THF solution of **1-Ce** with a 390 nm laser produces an emission band at 600 nm. Cyclic voltammetry (CV) experiments on **1-Ce** (see Section S4.1‡) at fast scan rates (ν = 0.5 V s^{-1}) display a quasi-reversible $Ce^{III/IV}$ redox couple at −0.15 V *vs.* $Fc^{0/+}$, Fig. 5 purple trace. The Rehm–Weller formalism (Section S4.2‡) predicts the $E_{1/2}$* of **1-Ce*** as −2.20 V. This value is similar to those calculated for Ce^{III} N-ligand complexes,[28] and more positive than the literature ground state $E_{1/2}$ of $PhCF_3$ (−3.23 V *vs.* $Fc^{0/+}$ in THF). This implies that the pre-coordination of the $PhCF_3$ to the Lewis acid Ln^{III} center is essential to provide the additional driving force.[28,64] See also the DFT calculations below.

Further CV measurements were performed to analyze the potentials and reversibility of the oxidations of complexes **2-Ce**, **1-La** and **2-La** as well as of the ligand **HL** (S4‡) in tetrabutylammonium tetraphenylborate [NBu_4][BPh_4] THF solutions.

In the case of **HL**, a redox peak around 0 V (*vs.* Fc/Fc^+) is observed upon scanning oxidatively, displaying partial reversibility upon increasing the scan speed. This can be explained by a slow, irreversible reaction of the oxidized ligand. A similar redox feature around −0.15 V is observed for **1-Ce**; the position of the oxidation at a more negative potential than that of free ligand implies a contribution from both the ligand and the metal center to this oxidation. This supports the hypothesis that electrons can be photoexcited from both metal and ligand.

In comparison, **1-La** shows an onset of oxidation of similar amplitude but around 0.15 V, close to the limit of the electrolyte stability window. There is also a smaller feature at −0.15 V, attributed to small amounts of free ligand that are released after the first oxidative scan of the bulk solution. **2-Ce** and **2-La** both display fully irreversible oxidations with onsets around −0.3 V and −0.05 V, respectively. The presence of additional redox features may indicate the formation of electrochemically active degradation products of the oxidation. The voltammograms of **2-La** and **2-Ce** have recently been reported and show that the oxidation of lanthanide tris-Cp^{Me4} complexes leads to decomposition at most standard scan rates.[65] Here in contrast, the oxidation of **1-Ce** is partially reversible at a scan rate of 500 mV s^{-1} (Fig. 5).

Stoichiometric C–F activation of $PhCF_3$ to afford $PhCF_2H$

First, complexes **1-Ce** to **6-Ce** were tested in a simple reaction with one equivalent of the substrate $PhCF_3$, Scheme 2. It is expected to proceed by homolytic C–F bond scission, with the $PhCF_2^{\bullet}$ subsequently abstracting a H atom from the solvent THF, a good H atom donor. Little conversion was seen in these reactions, hypothesized to be due to binding competition between $PhCF_3$ and THF solvent. Optimized reactions with five equivalents of $PhCF_3$ in THF solution, irradiated with a 40 W Kessil A160WE Tuna Blue lamp in a Young's tap-valved NMR tube, were then monitored by ^{19}F NMR spectroscopy.

Complex **1-Ce** performs best, forming the product $PhCF_2H$ in approximately 75% yield after 120 hours of irradiation at room temperature, Table S2.‡ The reaction does not proceed in the absence of light. Complex **2-Ce** which does not contain **L** makes $PhCF_2H$ in only 5% yield under the same conditions, underlining the utility of the aryloxy-NHC ligand. The La congener **1-La** is less effective than **1-Ce**, giving 10% conversion.

Prior to irradiation, the interaction between $PhCF_3$ and **1-Ln** found in the computational study is suggested by a small change in chemical shift in the ^{19}F NMR spectrum of $PhCF_3$ added to a solution of **1-La** or **1-Ce** compared to an isolated solution of $PhCF_3$ in a capillary, but chemical shifts in ^{19}F NMR spectroscopy can be very sensitive to concentration effects (Scheme 2 and S8.1, Fig. S97‡). This Lewis acid activation of the

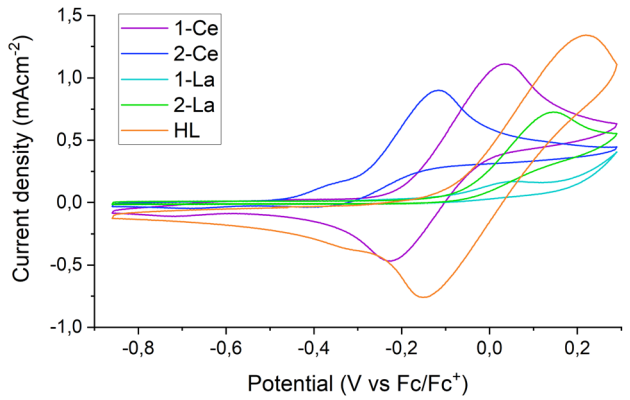

Fig. 5 Cyclic voltammograms of **1-Ce** (purple), **2-Ce** (dark blue), **1-La** (light blue), **2-La** (green) and **HL** (orange) in THF with 0.085 M [nBu_4N][BPh_4] supporting electrolyte. [Analyte] = *ca.* 5 mM; ν = 0.5 V s^{-1}.

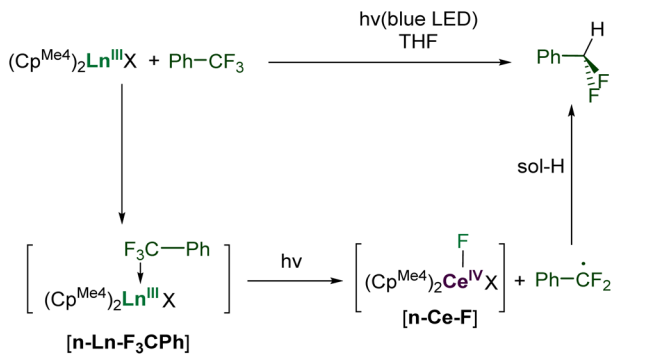

Scheme 2 General reaction scheme for C–F activation and hydrodefluorination by Ln complexes **1-Ln** to **3-Ln** and cleavage by the Ce photocatalysts **1-Ce**–**6-Ce** with $PhCF_3$ (X = the monoanionic ligand Cp^{Me4}, Cl, OAr, OTf, Bn) n = 1–3.

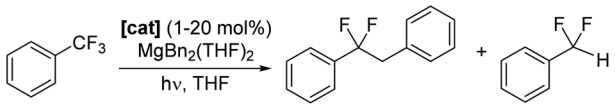

Scheme 3 Photocatalytic defluoroalkylation of trifluorobenzene with 1–6-Ce and $Mg(Bn)_2(THF)_2$.

C–F bond should facilitate its cleavage when the complex is photo-excited.

We expect the photoexcited adduct [**1-Ce–F_3CPh**] to fragment into the Ce^{IV}–F intermediate in Scheme 2, releasing the $PhCF_2^{\bullet}$ radical. Alternatively, the f^0 complex **1-La** can show hydrodefluorination reactivity by homolysis of one La–ligand bond under irradiation of [**1-La–F_3CPh**], forming a radical La fragment that can formally abstract $F^{\bullet}$. While few prior examples exist, the photoinduced homolysis of Ln–C bonds has been reported.[18,66]

Catalytic defluoroalkylation of C(sp^3)–F bonds: conversion of $PhCF_3$ to $PhCF_2CH_2CH_2R$

Photocatalysts **1–6-Ce** can also facilitate defluoroalkylation, using commonly available Mg dialkyls as both the source of alkyl group and fluoride acceptor to turn over the catalyst, Scheme 3. $MgBn_2(THF)_2$ [46] gives the most effective alkylation of the $ArCF_2^{\bullet}$ and is therefore used in the reactions described here. Products were identified as $PhCF_2R$ (R = H, Bn) by GC/MS and ^{19}F NMR spectroscopy, with minor amounts of the by-product $PhCF_2H$ and bibenzyl observed, presumably formed *via* homocoupling of benzyl radical.

Catalytic alkylation/arylation reactions are also possible using coupling partners $Mg(allyl)_2$, $MgPh_2(THF)_2$, or $^nBu_3Sn(allyl)$, (S6.2‡). Control reactions are described in Section S8.‡

Table 1 Defluoroalkylative coupling of $PhCF_3$ with $MgBn_2(THF)_2$ catalyzed by 20 mol% loading Ln or Mg photocatalyst[a]

Entry	Catalyst	Time (h)	Yield[b] (%)
1	**1-Ce**	48	51
2	**1-Ce**	80	91
3	**2-Ce**	48	6
4	**4-Ce**	48	41
5	**4-Ce**	80	65
6	**1-La**	48	67
7	**1-La**	60	72
8	**2-La**	48	19
9	**1-Nd**	48	32
10	**1-Nd**	140	87
11	**1-Sm**	48	12
12	**7-Mg**	48	24
13	**7-Mg**	80	56
14	None	260	22

[a] 20 mol% catalyst loading, 1 equiv. $MgBn_2(THF)_2$ and 1 equiv. $PhCF_3$, RT, THF-H_8, irradiation with a 40 W Kessil A160WE Tuna Blue lamp. [b] Combined yield of $PhCF_2CH_2Ph$ and $PhCF_2H$.

1-Ce is the best of the Ce photocatalysts, giving 91% conversion to product after a total of 80 hours irradiation (Table 1). The series **1-Ln** Ln = La, Ce, Nd, Sm was also tested using the same reaction conditions. After 48 hours irradiation all formed products, with yields that decrease from 67% for La to 13% for Sm, in alignment with decreasing atomic radius of the lanthanide. This is consistent with a mechanism that relies on substrate binding to the photoactivated complex and light absorption by the ligand **L** as well as (or instead of) the metal.

There is a very small amount of transfer of **L** from Ce to Mg during the catalysis with **1-Ce** observed by ^1H NMR spectroscopy, forming $[MgBn(\mathbf{L})]_2$ (**7-Mg**),[67] which we have independently synthesized. We note that **7-Mg** can also generate $ArCF_2^{\bullet}$ by F abstraction, in a similar manner to **1-La**. In catalysis, **7-Mg** forms a mixture of products in 56% yield after 80 hours irradiation. The bis(ligand) complex $[Mg(\mathbf{L})_2]_2$ (**8-Mg**) (see ESI‡) is much less reactive, presumably due to the greater steric crowding relative to **7-Mg**.

Some transfer of benzyl anion from the reagent $MgBn_2(THF)_2$ to **2–5-Ce** is also observed over time, with a gradual conversion to **6-Ce** as the reactions progress, see Fig. S113.‡ This ligand exchange is more significant for **2–5-Ce** than **1-Ce**, the most robust catalyst.

We also targeted the group 2 analogue [CaBn(**L**)] since Ca^{II} has a similar ionic radius to Ln^{III} ($r_{cov\ 6\ coordinate}$ Ce = 1.15; Ca = 1.14; Nd = 1.123 Å)[68] and would provide a catalyst with similar Lewis acidity but much less accessible d-orbitals at the metal. However, Schlenk equilibria prevented the isolation of a pure complex that could inform the mechanistic studies.

The conversion of $PhCF_3$ to $PhCF_2CH_2Ph$ can be catalyzed at catalyst loadings as low as 1 mol%. Table 2, and Fig. S69‡ show the data for the catalyzed conversion of $PhCF_3$ to $PhCF_2CH_2Ph$ in THF-H_8, mediated by 1 mol% loading of **1-Ce**, **1-La**, **1-Nd**, **1-Sm** or **7-Mg**. Following 63 hours irradiation, **1-Ce** produces a combined yield of 28% with a $PhCF_2CH_2Ph$: $PhCF_2H$ ratio of 5 : 1. **1-La** yields 42% conversion to $PhCF_2CH_2Ph$ and $PhCF_2H$ after 63 hours irradiation, which increases to 62% following a further 21 hours, albeit with a product ratio of 2 : 1.

Significantly, although **1-La** lacks the accessible metal-based $4f^1/5d^1$ excitation or III/IV redox couple, it can defluoroalkylate

Table 2 Defluoroalkylative coupling of $PhCF_3$ with $MgBn_2(THF)_2$ catalyzed by 1 mol% loading **1-Ln** or **7-Mg**[a]

Entry	Catalyst	Time (h)	Turnover	Ratio[b]
1	**1-Ce**	63	28	5 : 1
2	**1-La**	63	42	
3	**1-La**	84	62	2 : 1
4	**1-Nd**	63	20	3 : 1
5	**1-Sm**	63	21	3 : 1
6	**7-Mg**	63	23	
7	**7-Mg**	84	27	2 : 1

[a] 1 mol% catalyst loading, 1 equiv. $MgBn_2(THF)_2$ and 1 equiv. $PhCF_3$, RT, THF-H_8, irradiation with a 40 W Kessil A160WE Tuna Blue lamp; data at 84 hours unable to be collected for **1-Ce**, **1-Nd** and **1-Sm** due to polymerization of THF solvent. [b] Ratio of $PhCF_2CH_2Ph$ and $PhCF_2H$ products.

$PhCF_3$ faster than **1-Ce**. However, **1-Ce** is more selective in this transformation, capable of giving higher ratio of $PhCF_2CH_2Ph$ to $PhCF_2H$ than **1-La** (see Table 2).

There appears to be a large kinetic isotope effect in these reactions as the formation of $PhCF_2D$ as a side-product is suppressed in THF-D_8. For example, the ratio of $PhCF_2CH_2Ph$: $PhCF_2H$ formed by **1-Ce** improves from 5 : 1 in THF-H_8 to 11 : 1 in THF-D_8.

Additional experiments in which mixtures of **1-Ce** and $PhCF_3$ are irradiated with lower energy light (525 nm) give significantly lower yields of $PhCF_2H$ in agreement with our expectation that the higher energy absorption of **1** gives most efficient access to the photoexcited state. However, further reactions of **1-La** illuminated with the higher-energy 390 nm light result only in rapid decomposition of the lanthanum complex, Fig. S106.‡

Computational analysis of $PhCF_3$ binding and C–F bond homolysis

Computational approaches (DFT, B3PW91 functional) were again used to gain insight into the $PhCF_3$ coordination and C–F bond activation. The reaction, shown in Scheme 2, is calculated to begin by the photoexcitation of the **1-Ce** ground state to **1-Ce***, a transition which is calculated to be 81.3 kcal mol^{-1}, since the $PhCF_3$ coordination is weak. This corresponds to absorption of a 350 nm photon. From this intermediate, a transition state (TS1) was located on the Potential Energy Surface (PES) that corresponds to C–F activation of the $PhCF_3$ substrate, Fig. 6. The associated barrier from **1-Ce** is high (125.7 kcal mol^{-1}); that is, 44.4 kcal mol^{-1} from the photoexcited Ce^{III} state, **1-Ce***. The TS1 was located on the doublet spin state surface and Natural Population Analysis (NPA) shows TS1 is clearly a transfer of fluoride rather than fluorine radical, Scheme 4. The charge of the transferred F is −0.94, consistent with a fluoride. Concurrently, the charge at the Ce center is +3.85, in line with the formation of Ce(IV) center. This is similar to that demonstrated by 1,2,4-(^{t}Bu)$_3$-(C_5H_2)$_2$CeH in which Ce abstracts an F from Ce-bound CH_nF_{3-n} to form Ce–F + CH_nF_{2-n} radical.[63]

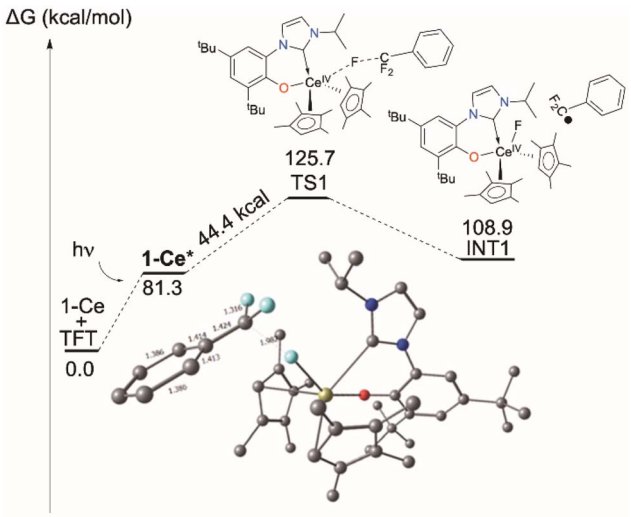

Fig. 6 Computed C–F activation pathway for the reaction of **1-Ce** with $PhCF_3$, including TS1. Those for **1-La** and **7-Mg** are in the ESI.‡

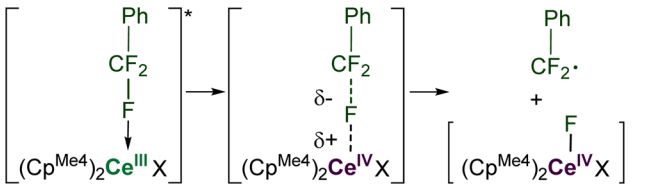

Scheme 4 Pathway for the abstraction of fluoride (rather than F$^\bullet$) to generate Ce(IV)–F and $ArCF_2^\bullet$.

Following the intrinsic reaction coordinate (IRC) leads to the formation of a Ce^{IV}–F complex (**INT1**) and free $PhCF_2^\bullet$ which is endothermic by 28.2 kcal mol^{-1} from the photoexcited **1-Ce*** state. The formation of the product $PhCF_2H$ *via* hydrogen atom abstraction from the solvent THF is computed to be athermic. This mechanism is distinct from the associative interchange process previously calculated for the reaction of $(Cp')_2CeCH_2Ph$ ($Cp' = 1,2,4$-tri-*t*-butylcyclopentadienyl) with methyl halides.[62]

The triplet transition state TS1 computed for the d^0f^0 **1-La** analogue, shown in the ESI,‡ is only 7.9 kcal above the **1-La*** excited state energy. The barrier for the excited state of the Mg^{II} complex **7-Mg***, also in the ESI,‡ is around 35 kcal mol^{-1} so that the reaction can occur but should be relatively slow, especially since the overall reaction is endothermic by 11.4 kcal mol^{-1}. The reaction energy could also be rendered exothermic by trapping the TFT radical by another molecule of **7-Mg*** or $MgBn_2(THF)_2$. The low barrier calculated for the **1-La** reaction corresponds less well to the observed reactivity, so it may be that the light absorption probability for **1-La** is lower, since it involves a form of ligand-to-ligand charge transfer that may well be dipole forbidden.

Experimental evidence for the formation of an $ArCF_2^\bullet$ radical intermediate

Seeking experimental support for the formation of a discrete $PhCF_2^\bullet$ intermediate, we prepared *ortho*-allylbenzotrifluoride 1-CF_3-2-(C_3H_5)C_6H_4 (**9**),[69] hypothesizing that the pendant alkene group would serve as an intramolecular radical trap for the proposed $ArCF_2^\bullet$ aryl radical. Irradiating a THF solution of **1-Ce** and **9** results in the slow formation of one major new product, assigned based on its ^{19}F NMR spectroscopic data, and comparison with an independently synthesized sample, Section

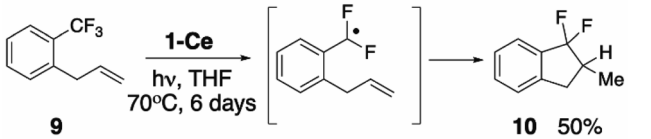

Scheme 5 The C–F bond activation of 1-CF_3-2-(C_3H_5)C_6H_4 mediated by **1-Ce**.

S8.2,‡ as the ring-closed **10** (Scheme 5, S8.2‡). The distinctive ^{19}F NMR spectra show large $^{2}J_{F,F}$ coupling constants of 250 Hz. The reaction of **1-Ce** with **9** is significantly slower than with $PhCF_3$, which we attribute to the greater steric hindrance about the activated CF_3 group in **9**.

Oxidation of the metal and/or ligand

The formation of the $ArCF_2^{\bullet}$ catalyzed by **1-Ln** should lead to an oxidized F-containing intermediate, [**1-Ln–F**]. The redox active and innocent metals can achieve this in different ways, shown in Scheme 6. For **1-Ce** we expect the $Ce^{III/IV}$ redox couple to be involved, forming the fluoride intermediate Ce^{IV} $[Ce(F)(L)(Cp^{Me4}{}_2]$ **1-Ce-F**, although we recognize that oxidation on the L or Cp^{Me4} ligand is also possible. For **1-La** and the other lanthanides which must remain Ln^{III} we expect either $[Ln(F)(L^{\bullet})(Cp^{Me4})_2]$ or $[Ln(F)(L)(Cp^{Me4\bullet})(Cp^{Me4})]$. We assume **7-Mg** will form [Mg(F)(L$^{\bullet}$)(Bn)] or [Mg(F)(L)] and $^{\bullet}$Bn.

Cerium(IV) fluorides are uncommon and difficult to work with, and if a fluoride was formed in the catalytic cycle, we did not expect it would be isolable.[73] The chemical oxidation of **1-Ce** and **1-La** was targeted using XeF_2 or the hypervalent iodine reagent $PhICl_2$ which has previously been used with success in organometallic Ce^{IV} chemistry.[70–72] Reactions between **1-Ce** and $PhICl_2$ resulted in an immediate color change to the characteristic purple of molecular Ce^{IV} but the mixture soon bleaches to pale pink. The other reactions gave mixtures of products that could not be identified by NMR or IR spectroscopy, or separated by fractional crystallization. A reaction of **6-Ce** with BF_3 to target a Ce^{III}–F complex which we planned to oxidize, yielded only the BF_4 complex $[(Cp^{Me4})_2Ce(BF_4)(THF)]_2$ whose X-ray structure is included in the ESI.‡

Calculations show that Cp^{Me4} is spontaneously released as a radical from the La center upon oxidation (S10.3‡) and providing a possible reason for the instability of **1-La** in catalysis particularly when using higher energy lamps; there is also precedent for the homolysis of Ln–Cp bonds.[74] Section S10.4‡ shows how for photoexcited **1-La*** the unpaired spin density is mainly located at the O–NHC ligand, but localizes on the Cp ring and develops on the coordinated $PhCF_3$ approaching the C–F activation step, finishing with unpaired spin density on both the $PhCF_2^{\bullet}$ radical and the Cp ligand.

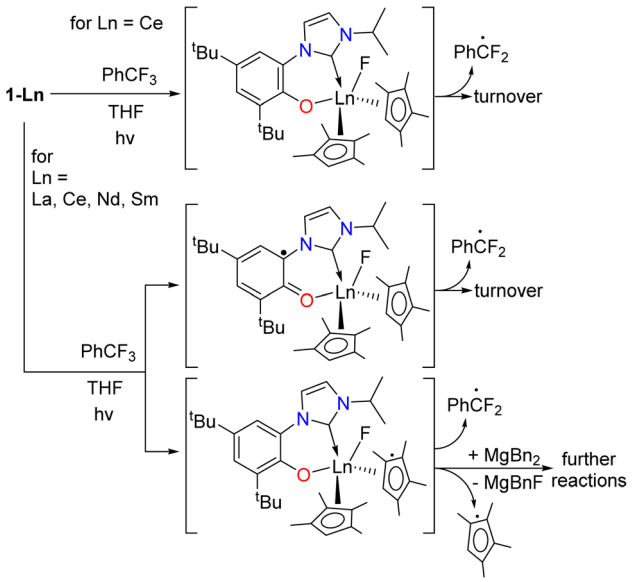

Scheme 6 The proposed pathways of oxidation of **1-Ln** that lead to turnover or catalyst degradation for Ln that have no accessible +IV oxidation state, *i.e.* Ln = La, Nd, and Sm.

The C–C bond forming step

Conventional organometallic Ce^{IV} alkyl complexes are not stable due to the reducing nature of the hydrocarbyl ligand.[71] In line with this, DFT calculations indicate that the formation of a discrete $[Ce^{IV}]$–Bn is energetically unfavorable, so we hypothesized that the C–C bond is formed by coupling of $ArCF_2^{\bullet}$ directly with the reagent $MgBn_2(THF)_2$. Intrinsic reaction coordinate (IRC) calculations on this coupling (Fig. 7) identify an achievable transition state at 16.3 kcal mol^{-1} above the ground state. We also calculated the alternative possibility in which **L** transfer to $MgBn_2(THF)_2$ generates **7-Mg** which we have observed as a by-product. Using the monomeric, THF-solvated form **7-Mg*** in the calculation, the barrier for this all-Mg mediated reaction, Fig. 8, is 3.5 kcal mol^{-1} higher. The transition state is 19.8 kcal mol^{-1} above the energy of **7-Mg*** and $PhCF_2^{\bullet}$.

The unpaired spin density rho (ρ) is reported on Fig. 7. As can be seen and as expected, the unpaired electron is first located on the $PhCF_2^{\bullet}$. At TS3, the simultaneous Mg–C bond breaking and the C–C bond formation suggests that the unpaired electron is delocalized between the $PhCF_2^{\bullet}$ and the Mg center. This clearly indicates that there is an homolytic cleavage of the Mg–C bond. This is further corroborated by the calculation showing that the unpaired spin density is localized at the Mg center in the final product. These results indicate that C–C bond formation is likely occurring at $MgBn_2(THF)_2$, which is

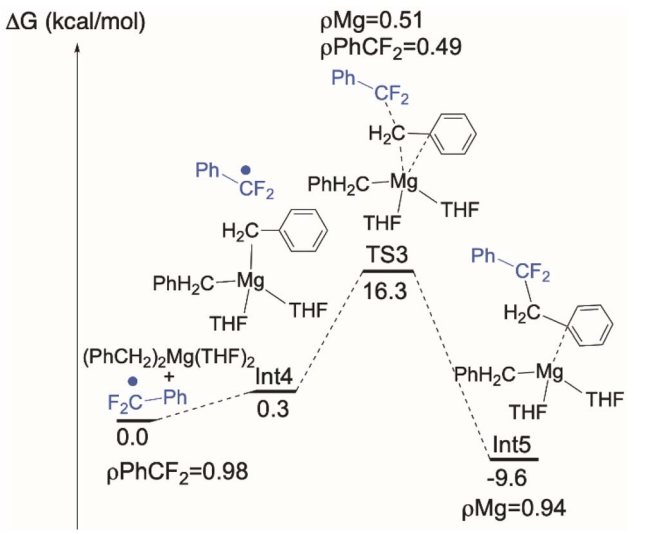

Fig. 7 Computed C–C coupling pathway at $MgBn_2(THF)_2$.

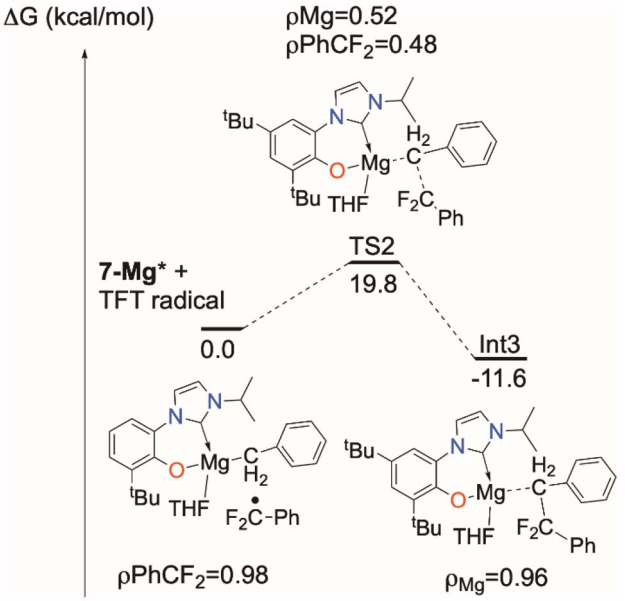

Fig. 8 Computed C–C coupling pathway at **7-Mg**.

also at significantly higher concentrations than **7-Mg** in solution during catalysis.

Mechanistic discussion

The reactivity described here is notable in that it is not limited to Ce, which is the only rare earth with an accessible (III/IV) redox couple and f–d orbital transition. It is these properties that have led to the recent and widespread interest in photoredox catalysis with Ce complexes. Of all the complexes that are capable catalysts described here, the Ce congener shows the longest catalyst life, and cleanest product formations. We suggest that this is because for the photoactivated $Ce^{III/IV}$ system there is a simple, metal-based process for redox shuttling that enables the fluoride to be captured and removed, as well as the opportunity for both ligand and metal orbitals to contribute to the light absorption and bonding of the complex. For La and other metals, the redox part of the cycle relies on the redox reactivity of an ancillary ligand. The involvement of both phenoxide and cyclopentadienyl ligands in redox reactions has been previously documented,[57–59,66,74] and cyclic voltammetry (CV) experiments show that pure **HL** possesses a pseudo-reversible redox event.

Our proposed mechanism is outlined in Scheme 7. First, a weak but observable interaction between a fluoride of $PhCF_3$ and the Ln metal, as observed in ^{19}F NMR experiments for both Ce and La, serves to bring the substrate into the active site. C–F → Ln^{III} (Ln = La, Sm, Yb) interactions have previously been hypothesized in the functionalization of C–F bonds mediated by lanthanide complexes.[37–39]

Photoexcitation to a more reducing excited state[3,75] follows, which leads to C–F cleavage and the generation of an $ArCF_2$ radical, as supported by experiments with a radical trapping substrate, Scheme 4. The nature of the resulting putative Ln–F species depends on the identity of the rare earth element. For Ce, a discrete Ce^{IV} species is the most likely intermediate. For La, the ligands (either **L** or Cp^{Me4}) serve as the electron source through ligand-based redox non-innocence.

Calculations suggest that the ease of M–Cp^{Me4} bond homolysis is greater for La *versus* Ce, and CV experiments imply that loss of a Cp^{Me4} ligand from **1-La** may lead to a cascading degradation process where the release of radical fragments accelerate decomposition (see Section S4‡). This supports the observation that complex **1-Ce** is more effective for C–F activation while complex **1-La** is faster for the coupling of the radical to form benzylated product, acting as a source of radicals that can facilitate C–F bond cleavage at the coordinated substrate. Moreover, **1-Ce** is the most thermally robust of **1-Ln**, able to operate at elevated temperatures (70 °C).

Reduction likely occurs when the generated $PhCF_2^{\bullet}$ couples with $MgBn_2$ to form the C–C bond, with the resulting transient Mg(I) complex serving to reduce either the metal (in the case of Ce) or the ligand (in the case of La) back to the initial catalytic species.

Calculations agree with the proposed mechanism and with the need for inner-sphere binding of the fluorinated substrate to Lewis acidic metal to provide sufficient weakening of the C–X bond to enable photochemical cleavage. They also show how the ligands can contribute to light absorption to generate the reactive excited state, and how oxidation of the complex can be localized on the metal (for Ce) or ligand (for the other metals) to enable turnover.

The NHC ligand **L** is not labile in this system;[16,76,77] variable temperature ^1H NMR spectra, see S8.9,‡ do not show any interactions between the NHC of **1-Ce** and $MgBn_2(THF)_2$ in THF solutions and all computed barriers increase in energy where the NHC is unbound or ligates to Mg or another reagent. Unsurprisingly, the calculations do not support the presence of a [Ce^{IV}–Bn] complex at any point.

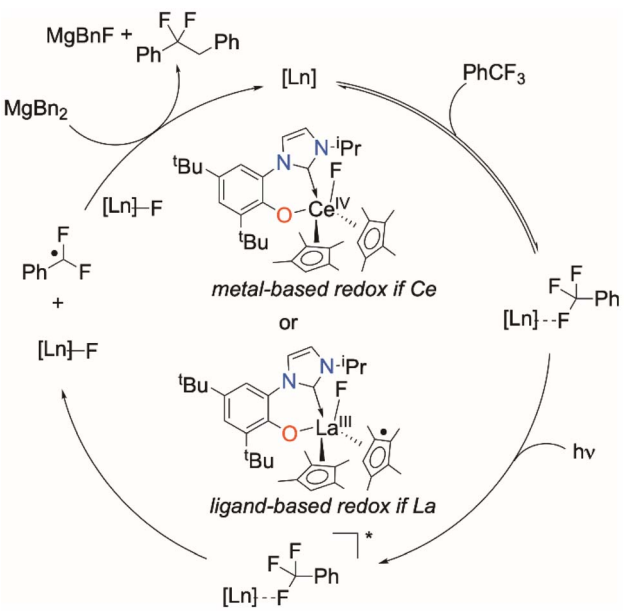

Scheme 7 Proposed mechanism of photocatalytic C–C coupling.

Conclusions

Cleavage and functionalization of the strong and inert sp^3 C–F bond of $PhCF_3$ can be readily achieved using single component, earth-abundant organometallic photocatalysts, requiring both the Lewis acidity of the metal to bind the substrate, and the visible light-absorbing capabilities of the rigid aromatic ligands. The reactivity described here is notable in that it is not limited to Ce, which has been the focus of a recent surge of interest in earth-abundant metal photocatalysts.

The photochemical hydrodefluorination and defluoroalkylation of $PhCF_3$ is feasible for typically photoinactive metals including La and Mg because the rigid aryloxy-NHC ligand facilitates visible light absorption. Experiments with a radical-trapping substrate support the formation of $ArCF_2$ radicals after C–F bond activation, and catalytic turnover in C–C bond forming reactions is most readily achieved using reagents such as $MgBn_2(THF)_2$ which can provide both the alkyl group and reduction of the catalyst intermediate. Computational experiments highlight the synergy between ligand-based and metal-based orbitals in the photoexcitation process. The complexes tested are also capable for homogeneous C(sp^3)–Cl bond activation and functionalization. Studies to increase the rates and scope of the reactivity of these systems, and further tuning of ligand- and metal-based absorptions in photocatalysts are currently underway in our laboratory.

Data availability

Additional experimental, computational, and crystallographic data (PDF) are in the ESI.‡ The crystallographic cif data are deposited with the CCDC, codes 2121204–2121215 and 2217133. Raw datasets are in the open data archive DOI: **10.17632/8bx8zxbdgm.1**.

Author contributions

A. E. K.: investigation (experimental), visualization, analysis, writing – original draft, review & editing. L. K. E.: investigation (experimental). A. N. D.: investigation (experimental), visualization, analysis, writing – original draft, review & editing. Y. Y.: investigation (computation). L. S.: investigation (cyclic voltammetry), analysis, writing – original draft. A. D. G.: investigation (experimental). T. D. T.: funding aquisition, supervision. L. M.: funding acquisition, supervision, analysis, writing – review & editing. P. L. A.: funding acquisition, supervision, visualization, analysis, writing – original draft, review & editing.

Conflicts of interest

There are no conflicts to declare.

Acknowledgements

The synthetic, catalytic, and crystallographic parts of this research were supported by the U.S. Department of Energy (DOE), Office of Science, Office of Basic Energy Sciences, Chemical Sciences, Geosciences, and Biosciences Division at the Lawrence Berkeley National Laboratory under Contract DE-AC02-05CH11231. The Catalysis Laboratory in the DOE Catalysis Program also provided resource for instrumentation used in this work. We also thank the University of Edinburgh. This project has received funding from the European Research Council (ERC) under the European Union's Horizon 2020 research and innovation programme (grant agreement No. 740311, P. L. A.) and the EPSRC are acknowledged for research funding through the UK Catalysis Hub (EP/K014714/1, P. L. A.). We acknowledge the National Institutes of Health (NIH) for funding the UC Berkeley College of Chemistry NMR facility under grant no. SRR023679A, S10OD024998 and 1S10RR016634-01, and Beamline 12.2.1 of the Advanced Light Source, which is a DOE Office of Science User Facility under contract no. DE-AC02-05CH11231. L. M. is a senior member of the Institut Universitaire de France. The Chinese Academy of Science and the Chinese Scholarship Council are acknowledged for financial support and CALMIP is thanked for a generous grant of computing time. The authors thank Rex C. Handford, Francis Y. T. Lam, Nicholas J. Katzer, Gabe Herrera, Dr Amy N. Price and Dr Anthony R. Wong for crystallographic and/or experimental help, as well as Prof. Rebecca J. Abergel, Dr Leticia Arnedo Sanchez and Dr Jennifer Wacker for help with photophysical measurements and Mr Gabriel Herrera for the LCMS and HRMS data.

References

1 G. E. M. Crisenza and P. Melchiorre, *Nat. Commun.*, 2020, **11**, 8–11.
2 J. W. Tucker and C. R. J. Stephenson, *J. Org. Chem.*, 2012, **77**, 1617–1622.
3 J. Twilton, C. Le, P. Zhang, M. H. Shaw, R. W. Evans and D. W. C. MacMillan, *Nat. Rev. Chem.*, 2017, **1**, 0052.
4 K. P. Shing Cheung, S. Sarkar and V. Gevorgyan, *Chem. Rev.*, 2022, **122**, 1543–1625.
5 D. Mazzarella, G. E. M. Crisenza and P. Melchiorre, *J. Am. Chem. Soc.*, 2018, **140**, 8439–8443.
6 D. T. Ahneman and A. G. Doyle, *Chem. Sci.*, 2016, **7**, 7002–7006.
7 A. Hu, J. J. Guo, H. Pan and Z. Zuo, *Science*, 2018, **361**, 668–672.
8 Z. Zuo, D. T. Ahneman, L. Chu, J. A. Terrett, A. G. Doyle and D. W. C. Macmillan, *Science*, 2014, **345**, 437–440.
9 B. Schweitzer-Chaput, M. A. Horwitz, E. de Pedro Beato and P. Melchiorre, *Nat. Chem.*, 2019, **11**, 129–135.
10 G. Goti, B. Bieszczad, A. Vega-Peñaloza and P. Melchiorre, *Angew. Chem., Int. Ed.*, 2019, **58**, 1213–1217.
11 C. Le, T. Q. Chen, T. Liang, P. Zhang and D. W. C. MacMillan, *Science*, 2018, **360**, 1010–1014.
12 S. T. Nguyen, P. R. D. Murray and R. R. Knowles, *ACS Catal.*, 2020, **10**, 800–805.
13 Y. Zhou, D. Hu, D. Li and X. Jiang, *JACS Au*, 2021, **1**, 1141–1146.
14 J. J. Guo, A. Hu, Y. Chen, J. Sun, H. Tang and Z. Zuo, *Angew. Chem., Int. Ed.*, 2016, **55**, 15319–15322.
15 T. Cheisson and E. J. Schelter, *Science*, 2019, **363**, 489–493.
16 P. L. Arnold, R. W. F. Kerr, C. Weetman, S. R. Docherty, J. Rieb, F. L. Cruickshank, K. Wang, C. Jandl,

M. W. McMullon, A. Pöthig, F. E. Kühn and A. D. Smith, *Chem. Sci.*, 2018, **9**, 8035–8045.
17 R. W. F. Kerr, P. M. D. A. Ewing, S. K. Raman, A. D. Smith, C. K. Williams and P. L. Arnold, *ACS Catal.*, 2021, **11**, 1563–1569.
18 P. L. Watson, T. H. Tulip and I. Williams, *Organometallics*, 1990, **9**, 1999–2009.
19 T. Kondo, M. Akazome and Y. Watanabe, *J. Chem. Soc., Chem. Commun.*, 1991, 757.
20 A. Ogawa, S. Ohya, Y. Sumino, N. Sonoda and T. Hirao, *Tetrahedron Lett.*, 1997, **38**, 9017–9018.
21 T. C. Jenks, M. D. Bailey, J. L. Hovey, S. Fernando, G. Basnayake, M. E. Cross, W. Li and M. J. Allen, *Chem. Sci.*, 2018, **9**, 1273–1278.
22 J. Ma, F. Schäfers, C. Daniliuc, K. Bergander, C. A. Strassert and F. Glorius, *Angew. Chem., Int. Ed.*, 2020, **59**, 9639–9645.
23 N. Nensala and T. Nyokong, *Polyhedron*, 1997, **16**, 2971–2978.
24 M. D. Rausch, K. J. Moriarty, J. L. Atwood, J. A. Weeks, W. E. Hunter and H. G. Brittain, *Organometallics*, 1986, **5**, 1281–1283.
25 P. N. Hazin, J. W. Bruno and H. G. Brittain, *Organometallics*, 1987, **6**, 913–918.
26 H. Yin, P. J. Carroll, J. M. Anna and E. J. Schelter, *J. Am. Chem. Soc.*, 2015, **137**, 9234–9237.
27 Y. Qiao and E. J. Schelter, *Acc. Chem. Res.*, 2018, **51**, 2926–2936.
28 H. Yin, P. J. Carroll, B. C. Manor, J. M. Anna and E. J. Schelter, *J. Am. Chem. Soc.*, 2016, **138**, 5984–5993.
29 H. Yin, Y. Jin, J. E. Hertzog, K. C. Mullane, P. J. Carroll, B. C. Manor, J. M. Anna and E. J. Schelter, *J. Am. Chem. Soc.*, 2016, **138**, 16266–16273.
30 A. Prieto and F. Jaroschik, *Curr. Org. Chem.*, 2022, **26**, 6–41.
31 Y. Qiao, Q. Yang and E. J. Schelter, *Angew. Chem., Int. Ed.*, 2018, **57**, 10999–11003.
32 S. J. Gray, K. Brown, F. Y. T. Lam, J. A. Garden and P. L. Arnold, *Organometallics*, 2021, **40**, 948–958.
33 F. Sinclair, J. A. Hlina, J. A. L. Wells, M. P. Shaver and P. L. Arnold, *Dalton Trans.*, 2017, **46**, 10786–10790.
34 B. E. Smart, in *Organofluorine Chemistry: Principles and Commercial Applications*, ed. R. E. Banks, B. E. Smart and J. C. Tatlow, Springer US, Boston, MA, 1994, pp. 57–88.
35 Y. Wang and A. Liu, *Chem. Soc. Rev.*, 2020, **49**, 4906–4925.
36 T. Ahrens, J. Kohlmann, M. Ahrens and T. Braun, *Chem. Rev.*, 2015, **115**, 931–972.
37 M. Janjetovic, A. M. Träff, T. Ankner, J. Wettergrena and G. Hilmersson, *Chem. Commun.*, 2013, **49**, 1826–1828.
38 A. M. Träff, M. Janjetovic, L. Ta and G. Hilmersson, *Angew. Chem., Int. Ed.*, 2013, **52**, 12073–12076.
39 M. Janjetovic, A. M. Träff and G. Hilmersson, *Chem.–Eur. J.*, 2015, **21**, 3772–3777.
40 F. Tian, G. Yan and J. Yu, *Chem. Commun.*, 2019, **55**, 13486–13505.
41 H. Iwamoto, H. Imiya, M. Ohashi and S. Ogoshi, *J. Am. Chem. Soc.*, 2020, **142**, 19360–19367.
42 X. Gong, Q. Zhou and G. Yan, *Org. Biomol. Chem.*, 2022, **20**, 5365–5376.
43 Y. J. Yu, F. L. Zhang, T. Y. Peng, C. L. Wang, J. Cheng, C. Chen, K. N. Houk and Y. F. Wang, *Science*, 2021, **371**, 1232–1240.
44 J. B. I. Sap, N. J. W. Straathof, T. Knauber, C. F. Meyer, C. F. Meyer, M. Médebielle, L. Buglioni, C. Genicot, A. A. Trabanco, T. Noël, C. W. Am Ende and V. Gouverneur, *J. Am. Chem. Soc.*, 2020, **142**, 9181–9187.
45 Y. C. Luo, F. F. Tong, Y. Zhang, C. Y. He and X. Zhang, *J. Am. Chem. Soc.*, 2021, **143**, 13971–13979.
46 C. Luo and J. S. Bandar, *J. Am. Chem. Soc.*, 2019, **141**, 14120–14125.
47 D. Mandal, R. Gupta, A. K. Jaiswal and R. D. Young, *J. Am. Chem. Soc.*, 2020, **142**, 2572–2578.
48 G. Yan, *Chem.–Eur. J.*, 2022, **28**, e202200231.
49 G. Yan, K. Qiu and M. Guo, *Org. Chem. Front.*, 2021, **8**, 3915–3942.
50 D. B. Vogt, C. P. Seath, H. Wang and N. T. Jui, *J. Am. Chem. Soc.*, 2019, **141**, 13203–13211.
51 H. Wang and N. T. Jui, *J. Am. Chem. Soc.*, 2018, **140**, 163–166.
52 K. Chen, N. Berg, R. Gschwind and B. König, *J. Am. Chem. Soc.*, 2017, **139**, 18444–18447.
53 N. Sugihara, K. Suzuki, Y. Nishimoto and M. Yasuda, *J. Am. Chem. Soc.*, 2021, **143**, 9308–9313.
54 P. Pinter, C. M. Schüßlbauer, F. A. Watt, N. Dickmann, R. Herbst-Irmer, B. Morgenstern, A. Grünwald, T. Ullrich, M. Zimmer, S. Hohloch, D. M. Guldi and D. Munz, *Chem. Sci.*, 2021, **12**, 7401–7410.
55 H. Yamashita, T. Ikezawa, Y. Kobayashi and J. Abe, *J. Am. Chem. Soc.*, 2015, **137**, 4952–4955.
56 J. Li, C. Huang and C. Li, *Chem*, 2022, 1–13.
57 S. Shirase, K. Shinohara, H. Tsurugi and K. Mashima, *ACS Catal.*, 2018, **8**, 6939–6947.
58 M. R. Ringenberg, S. L. Kokatam, Z. M. Heiden and T. B. Rauchfuss, *J. Am. Chem. Soc.*, 2008, **130**, 788–789.
59 L. Benisvy, A. J. Blake, D. Collison, E. S. Davies, C. D. Garner, E. J. L. McInnes, J. McMaster, G. Whittaker and C. Wilson, *Dalton Trans.*, 2003, 1975–1985.
60 V. F. Quiroga Norambuena, A. Heeres, H. J. Heeres, A. Meetsma, J. H. Teuben and B. Hessen, *Organometallics*, 2008, **27**, 5672–5683.
61 E. L. Werkema, L. Castro, L. Maron, O. Eisenstein and R. A. Andersen, *New J. Chem.*, 2013, **37**, 132–142.
62 E. L. Werkema, R. A. Andersen, L. Maron and O. Eisenstein, *Dalton Trans.*, 2010, **39**, 6648.
63 L. Maron, E. L. Werkema, L. Perrin, O. Eisenstein and R. A. Andersen, *J. Am. Chem. Soc.*, 2005, **127**, 279–292.
64 H. Yin, A. V. Zabula and E. J. Schelter, *Dalton Trans.*, 2016, **45**, 6313–6323.
65 M. T. Trinh, J. C. Wedal and W. J. Evans, *Dalton Trans.*, 2021, **50**, 14384–14389.
66 M. E. Fieser, C. W. Johnson, J. E. Bates, J. W. Ziller, F. Furche and W. J. Evans, *Organometallics*, 2015, **34**, 4387–4393.
67 J. B. Waters and J. M. Goicoechea, *Dalton Trans.*, 2014, **43**, 14239–14248.
68 R. D. Shannon, *Acta Crystallogr., Sect. A: Cryst. Phys., Diffr., Theor. Gen. Crystallogr.*, 1976, **32**, 751–767.

69 P. Clavel, G. Lessene, C. Biran, M. Bordeau, N. Roques, S. Trévin and D. de Montauzon, *J. Fluorine Chem.*, 2001, **107**, 301–310.
70 P. Dröse, A. R. Crozier, S. Lashkari, J. Gottfriedsen, S. Blaurock, C. G. Hrib, C. Maichle-Mössmer, C. Schädle, R. Anwander and F. T. Edelmann, *J. Am. Chem. Soc.*, 2010, **132**, 14046–14047.
71 R. Anwander, M. Dolg and F. T. Edelmann, *Chem. Soc. Rev.*, 2017, **46**, 6697–6709.
72 D. Schneider, N. Harmgarth, F. T. Edelmann and R. Anwander, *Chem.–Eur. J.*, 2017, **23**, 12243–12252.
73 U. J. Williams, J. R. Robinson, A. J. Lewis, P. J. Carroll, P. J. Walsh and E. J. Schelter, *Inorg. Chem.*, 2014, **53**, 27–29.
74 T. J. Mueller, M. E. Fieser, J. W. Ziller and W. J. Evans, *Chem. Sci.*, 2011, **2**, 1992–1996.
75 Y. H. Wang, Q. Yang, P. J. Walsh and E. J. Schelter, *Org. Chem. Front.*, 2022, 2612–2620.
76 Z. R. Turner, R. Bellabarba, R. P. Tooze and P. L. Arnold, *J. Am. Chem. Soc.*, 2010, **132**, 4050–4051.
77 I. J. Casely, S. T. Liddle, A. J. Blake, C. Wilson and P. L. Arnold, *Chem. Commun.*, 2007, 5037–5039.